

Magnesium AZ63 Alloy Protective Coatings by Plasma Electrolytic Oxidation in Mixed Aqueous Electrolytes

Ion Patrascu

Doctoral School Materials Science and Engineering, National University of Science and Technology POLITEHNICA Bucharest, Romania
patrascu@ipad.ro

Aurelian Denis Negrea

Regional Center of Research & Development for Materials, Processes and Innovative Products Dedicated to the Automotive Industry (CRCD-AUTO), National University of Science and Technology POLITEHNICA Bucharest, Romania
aurelian.negrea@upb.ro

Viorel Malinovschi

Department of Environmental Engineering and Applied Sciences, National University of Science and Technology POLITEHNICA Bucharest, Romania
viorel.malinovschi@upit.ro

Cristian Petrica Lungu

National Institute for Laser, Plasma and Radiation Physics, Romania
cplunguro@yahoo.co.uk

Ramona Cimpoesu

Faculty of Science and Material Engineering, "Gheorghe Asachi" Technical University of Iasi, Romania
ramona.cimpoesu@academic.tuiasi.ro

Marian Catalin Ducu

Faculty of Mechanics and Technology, National University of Science and Technology POLITEHNICA Bucharest, Romania
marian_catalin.ducu@upb.ro

Adriana-Gabriela Schiopu

Faculty of Mechanics and Technology, National University of Science and Technology POLITEHNICA Bucharest, Romania
gabriela.schiopu@upb.ro

Sorin Georgian Moga

Regional Center of Research & Development for Materials, Processes and Innovative Products Dedicated to the Automotive Industry (CRCD-AUTO), National University of Science and Technology POLITEHNICA Bucharest, Romania
sorin_georgian.moga@upb.ro (corresponding author)

Received: 20 March 2024 | Revised: April 2024 | Accepted: 11 April 2024

Licensed under a CC-BY 4.0 license | Copyright (c) by the authors | DOI: <https://doi.org/10.48084/etasr.7303>

ABSTRACT

Ceramic protective coatings, primarily composed of spinel (MgAl_2O_4), magnesia (MgO), and trimagnesium phosphate ($\text{Mg}_3(\text{PO}_4)_2$), were produced on magnesium AZ63 alloy through Plasma Electrolytic Oxidation (PEO) in mixed sodium phosphate/aluminate electrolytes with varying aluminate concentrations and constant processing time. The morpho-structural and compositional characteristics of the coatings were studied using X-ray diffraction, scanning electron microscopy, and energy-dispersive X-ray spectroscopy. Their functional mechanical and anti-corrosive properties were assessed through tribological testing, electrochemical impedance spectroscopy, and potentiodynamic bias tests. The findings indicated that the samples processed through PEO exhibited significantly enhanced properties compared to the AZ63 magnesium alloy. The best tribological properties were observed for the lowest aluminate concentration. Optimum corrosion resistance properties were obtained for coatings produced in a mixed electrolyte of 10 g/L sodium phosphate and 20 g/L sodium aluminate.

Keywords-plasma electrolytic oxidation; magnesium alloy; mixed electrolyte; tribological properties; anti-corrosive properties

I. INTRODUCTION

Plasma Electrolytic Oxidation (PEO) is an electrochemical surface treatment process used to create a thick, hard, and corrosion-resistant oxide layer on the surface of various metals or alloys, most notably based on light metals such as aluminum, magnesium, and titanium [1-3]. This process involves submerging the metal in an electrolyte solution and applying a high voltage. This creates a plasma discharge at the interface between the metal and the electrolyte, which breaks down the metal oxide and allows new oxide layers to form. The new oxide layer is much thicker and denser than the original oxide layer and is also much more adherent to the metal substrate [4]. PEO is a versatile process that can be employed to improve the performance of a wide variety of metal components utilized on pistons, cylinder lines, engine components, aircraft landing gears, and biocompatible implants [5-11]. Pure magnesium and some alloys are susceptible to corrosion, particularly in humid environments or saltwater, limiting their use in certain applications. Some alloys have relatively low wear resistance, which can be a drawback in applications involving friction and abrasion. Surface modifications, such as PEO, are crucial to address these limitations and enhance the overall usability of magnesium alloys. PEO treatment significantly improves the corrosion resistance and mechanical properties of magnesium and its alloys [12]. In [13], the influence of the processing time in aluminate electrolytes on the structure was studied along with the functional properties of PEO coatings on AZ63 magnesium alloy. The results showed that PEO processing improved the corrosion protective properties by two orders of magnitude and increased five times the Vickers micro-hardness of the surface, compared to the bare magnesium alloy. PEO processing of Mg AZ63 alloy in individual aluminate, phosphate, and silicate electrolytes with NaOH addition produced coatings with thicknesses up to 180 μm , with clearly improved functional properties compared to magnesium alloy [14].

Until now, some interesting results have been obtained for the processing through PEO of magnesium alloys in mixed phosphate/aluminate aqueous electrolytes. In [15], it was investigated how the addition of NaAlO_2 (ranging from 0 to 8 g/L) to a phosphate-based electrolyte (containing 10 g/L Na_3PO_4) with KOH (1 g/L) affected the properties of PEO coatings formed on AM60B magnesium alloy. The most

uniform coatings were obtained for the electrolyte without aluminate, whereas the coatings with the highest aluminate concentration exhibited the best anti-corrosive properties. In [16], the influence of phosphate concentration (0, 8.20, 12.30, and 16.40 g/L) in mixed aluminate/phosphate electrolytes with constant concentrations of $\text{K}_2\text{Al}_2\text{O}_4$ and NaOH as additives on the thickness and anti-corrosive properties of the coatings was examined. The results manifested that the thickness of the coatings increased with the phosphate concentration, but the best anti-corrosive properties were acquired for a concentration of 8.20 g/L sodium phosphate. In [17], the influence of different electrolyte concentrations based on phosphates, aluminates, and phosphate/aluminate mixtures with KOH as an additive was examined on the anti-corrosive properties of coatings obtained through PEO on the AM50 magnesium alloy. The thickest coatings were acquired for phosphate-based electrolytes, followed by mixed aluminate/phosphate and aluminate-based electrolytes. Simultaneously, the coatings obtained in mixed aluminate/phosphate electrolytes exhibited the highest impedance upon exposure to a 3.5% NaCl solution.

Within this framework, the current study aims to generate ceramic coatings on AZ63 magnesium alloys through PEO treatment using mixed $\text{NaAlO}_2/\text{Na}_3\text{PO}_4$ aqueous electrolytes at different concentrations of aluminate species and study the influence of the electrolyte composition on the structure, morphology, and functional properties of the AZ63 magnesium alloy PEO coatings. The innovative aspect of this method lies in employing this specific AZ63 alloy as the substrate for the development of PEO coatings in mixed electrolytes, while simultaneously emphasizing the enhancement of mechanical properties and corrosion resistance.

II. EXPERIMENTAL WORK

The Mg AZ63 alloy was cut into a 20 mm diameter and 4 mm thick discs. The latter were mechanically polished, cleaned in an ultrasonic bath in acetone, and then subjected to PEO in a custom-built installation described in [18]. The PEO conditions were: mixed $\text{NaAlO}_2/\text{Na}_3\text{PO}_4$ aqueous electrolytes, frequency 150 Hz, unipolar pulsed galvanostatic mode, current density 0.13 A/cm^2 , 25% average duty cycle, and constant processing time of 10 min. The maximum working voltage amplitude for all samples was about 450 V. Table I presents the composition and properties of the mixed aqueous electrolytes used for the PEO processing of three different Mg AZ63 alloy samples.

TABLE I. ELECTROLYTE CHARACTERISTICS

Sample	Electrolyte		
	Composition	pH	Electrical conductivity (mS/cm)
S1	10g/L Na ₃ PO ₄ + 15g/L NaAlO ₂	12.7	24.5
S2	10g/L Na ₃ PO ₄ + 20g/L NaAlO ₂	12.8	27.4
S3	10g/L Na ₃ PO ₄ + 25g/L NaAlO ₂	12.9	30.1

X-Ray Diffraction (XRD) data were recorded on a Rigaku Ultima IV diffractometer in Bragg-Brentano geometry, CuK_α radiation, utilizing a 1D D/teX Ultra detector with a graphite monochromator in the 2θ range [15-85°], step size of 0.02°, and a scan rate of 1°/min. XRD patterns were used to qualitatively and quantitatively evaluate the polycrystalline phases present in the investigated samples. Scanning Electron Microscopy coupled with Energy Dispersive X-ray Spectrometry (SEM-EDS) analysis of both the sample's surface and cross-section was performed with a Hitachi SU5000 scanning electron microscope in a low-vacuum mode. For the coated samples' surface roughness analysis, a 4-channel Back-Scattered Electron (BSE) detector system was deployed to generate the 3D models in the Hitachi Map 3D software. Porosity analysis was conducted utilizing ImageJ software for image processing and analysis on 3 sets of SEM images. For the cross-section PEO thin film analysis, the samples were cut, embedded in conductive resin, and gradually polished with abrasive papers with different grain sizes. A CSM (Swiss) ball-on disc tribometer was implemented to compute the behavior of the coefficient of friction as a function of the sliding distance. The hardness of the coating layers was measured perpendicularly on the film surface with a Vickers microhardness tester (Future-Tech FM 700) under an applied load of 0.5 kgf and a dwell time of 15 s. The adhesion strength of the prepared coatings was calculated using a Teer ST-30 scratch tester equipped with a 0.2 mm radius diamond tip. All corrosion experiments were carried out in a 100 ml three-electrode type cell at room temperature. The counter electrode was a platinum wire, whereas the working electrode was the sample with a surface of exposure to the corrosion environment equal to 0.5 cm². The reference was a saturated calomel electrode. The electrolytic solution was a 3.5% NaCl solution. An Orgaflex 01A workstation electrochemical device was put into service for all of the experiments. Data acquisition was performed with OrigaMaster 5 software, and the ZSimpWin software was employed to process the collected data. Potentiodynamic polarization curves were registered by sweeping the potential from the cathodic to the anodic direction. Before potentiodynamic polarization measurements, a stabilization period of 30 minutes was measured to register the Open Circuit Potential (OCP). For the linear anodic polarization - Tafel method, the potential range was -200 to 200 mV with respect to the open circuit potential, at a scan rate of 1 mV/s. Cyclic voltammetry measurements were performed in the range -0.2 to 0.7 V versus OCP, with a scan rate of 5 mV/s. Impedance spectroscopy measurements (EIS) were taken in the frequency range between 10 MHz and 100 KHz. The measurements were made using a 10 mV amplitude AC potential.

III. RESULTS AND DISCUSSIONS

A. XRD Analysis

Qualitative phase analysis was performed using the Rigaku PDXL 2 software and the ICDD PDF4+ 2023 database. Figure 1 portrays the XRD patterns and the qualitative phase analysis of both the Mg AZ63 alloy and the PEO-processed samples.

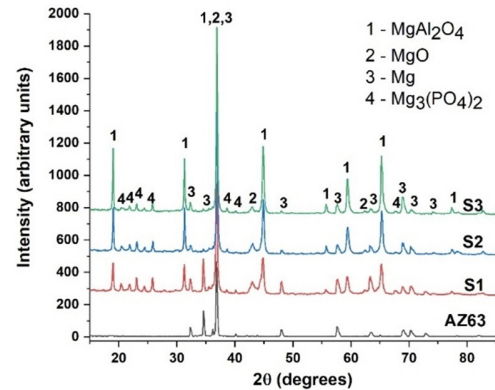


Fig. 1. XRD patterns and qualitative phase analysis.

In addition to the characteristic lines of the AZ63 Mg alloy substrate, all samples processed through PEO exhibit diffraction lines associated with magnesium compounds, typical for magnesium alloy PEO processing in aluminate/phosphate mixed electrolytes [16]. The reduction in the intensity of the diffraction lines associated with the α-Mg phase can be correlated with an increase in the thickness of the ceramic protective layer with an increase in sodium aluminate concentration from 15 to 25 g/L. Table II presents the results of the quantitative phase analysis, conducted adopting the Whole Powder Pattern Fitting (WPPF) method.

TABLE II. WPPF RESULTS

Sample	Quantitative phase composition (wt.±SD, %)			
	MgAl ₂ O ₄	MgO	Mg	Mg ₃ (PO ₄) ₂
S1	34.75 ±0.57	41.67 ± 3.86	11.45 ±0.41	12.13 ±1.13
S2	62.16 ±0.56	23.69 ± 0.56	5.08 ±0.27	9.09 ±0.87
S3	74.69 ±0.62	15.19 ±3.69	4.69 ±0.30	5.43 ±0.64

Table II depicts the variation of the polycrystalline phase concentrations of the PEO coatings with the electrolyte composition used to process the respective sample. As noted previously, the existence of aluminates in the solution encourages the creation of spinel, MgAl₂O₄ [12], such that a higher concentration of aluminate in the electrolyte will lead to the formation of layers with a higher concentration of MgAl₂O₄.

B. SEM-EDS Analysis

Figure 2 presents representative examples of the surface morphology of a PEO-treated sample in a mixed aqueous electrolyte, obtained by the backscattered electron - secondary electron SEM.

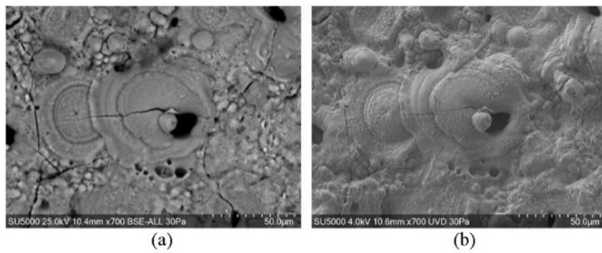


Fig. 2. Surface morphology of S3 sample obtained by SEM (×700 magnification) in (a) backscatter electrons and (b) secondary electrons.

Figure 2 illustrates a characteristic porous morphology with micro-cracks and re-solidified melt pools, typical to PEO-processed surfaces [19]. SEM-EDS area scans were performed to extract the chemical elemental concentrations of the PEO-obtained samples, as observed in Table III. The acquired data confirm that the PEO-obtained samples show oxide formations and the successful integration of species from the electrolyte. The chemical elemental composition of the Mg AZ63 alloy substrate is demonstrated elsewhere [13].

TABLE III. EDS CHEMICAL ELEMENTAL ANALYSIS

Element	S1 (wt. ± SD, %)	S2 (wt. ± SD, %)	S3 (wt ± SD, %)
Mg	21.44±0.11	19.57±0.11	18.51±0.11
Al	19.73±0.11	22.11±0.11	24.98±0.13
P	10.05±0.08	8.15±0.07	7.47±0.08
O	44.22±0.17	45.21±0.17	44.35±0.17
Si	0.13±0.03	0.06±0.03	0.09±0.04
Na	3.99±0.09	4.50±0.09	4.28±0.09
Mn	0.11±0.04	0.10±0.04	0.15±0.04
Zn	0.33±0.06	0.30±0.06	0.16±0.06

A correlation of the EDS results with the XRD data can be observed, with the Al concentration increasing on the surface with the concentration of aluminate in the electrolyte, whereas the concentration of P and Mg decreases. For the porosity analysis, considering the SEM micrographs resolution and the presence of image artifacts (e.g. surface cracks and micro-discharge channels), several analysis constraints were added: apparent pore size interval 10-100µm, circularity 0.2-1.0, and exclude pores on image edges. Figure 3 exhibits an example of pore size identification. Roughness analysis was performed using the Hitachi Map 3D software and 3 sets of 4 SEM images for each sample at ×200 magnification (Figure 4).

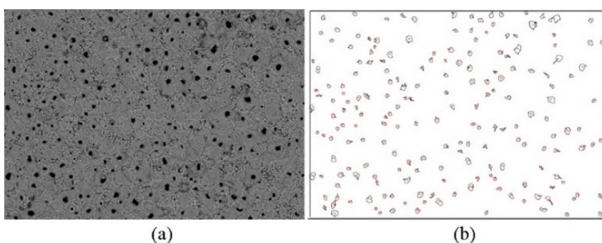


Fig. 3. Pore size identification for sample S2 (×100 magnification): (a) backscatter electron SEM image and (b) ImageJ pores analysis.

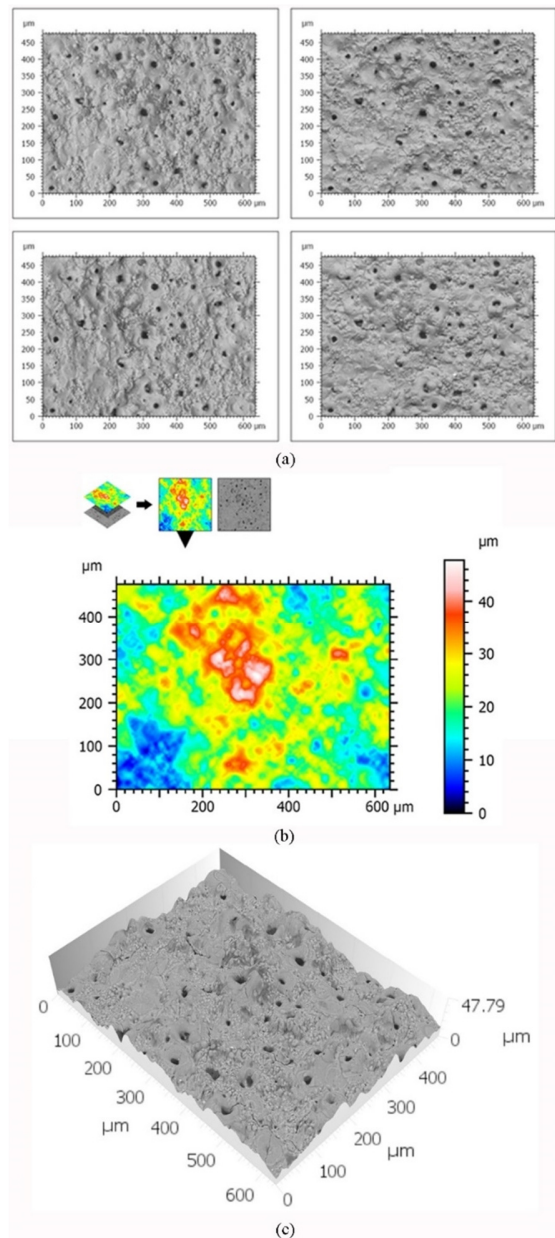


Fig. 4. Example of a 3D SEM-BSE topographical analysis performed on sample S3 (×200 magnification): (a) the four BSE images acquired on the same surface by the 4-channel BSE detector; (b) generated 2D surface height map and (c) 3D surface rendering.

Table IV displays the average surface porosity of the investigated samples, calculated as the ratio between the pores area and the total investigated surface area. The mean surface roughness values of the sample are also presented.

TABLE IV. SURFACE POROSITY AND ROUGHNESS OF PEO COATINGS

Sample code	Average surface porosity ± SD (%)	Average surface roughness ± SD (µm)
S1	3.99 ± 0.14	5.90 ± 0.59
S2	3.75 ± 0.04	5.98 ± 0.60
S3	2.98 ± 0.07	6.09 ± 0.61

The results showcased in Table IV disclose only slight differences in the average surface porosity and roughness from sample S1 to S3, which might suggest that the increase in the NaAlO₂ concentration (from 15 to 25 g/l) within the electrolyte solution with constant PEO processing time (10 min) does not significantly influence those surface characteristics. Coating thickness measurements were taken in cross-section by scanning electron microscopy. For each sample, 3 different random cross-section micrographs (×200 mag.) were acquired, and for each of them, the PEO coating thickness was measured in 5 different places. Figure 5 provides a representative example for each sample, and the mean values are presented in Table V.

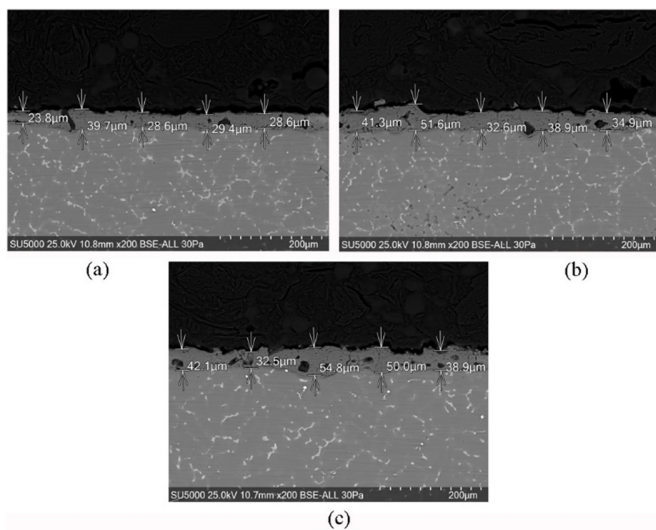


Fig. 5. Example of cross-section PEO coating thickness measurements by SEM (×200 magnification) for samples S1 (a), S2 (b), and S3 (c).

TABLE V. PEO COATING THICKNESS

Sample code	Mean coating thickness ± SD (µm)
S1	34.48 ± 9.57
S2	39.34 ± 8.44
S3	46.25 ± 11.91

The data portrayed in Table V indicate an increase in the coating thickness with an increase in the aluminate concentration in the electrolyte. Figure 6 illustrates the cross-section line-scan analysis performed at 1K magnification. The SEM micrographs exhibit a cross-section structure containing a barrier layer at the interface between AZ63 bulk and PEO coating, open pores, closed pores, and smaller inner voids together with discharge channels. The EDS analysis manifests a relatively uniform elemental cross-section dispersion in the PEO coating with Mg, Al, and O as the main elements.

C. Tribology Measurements

To determine the friction coefficient behavior, a normal load of 2N was applied on a static partner made of a sapphire 6 mm in diameter. A 3 mm radius and a sliding speed of 2 cm/s were used. The sliding distance was settled at 25 m. The specific wear rate was determined based on the relationship among the volume loss of the material after wear (mm³), the normal load applied (N), and the sliding distance (m) [20].

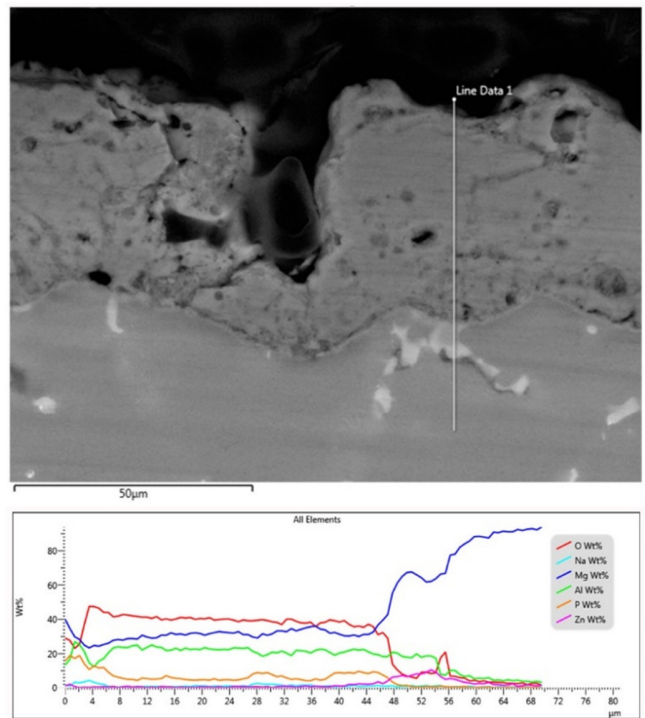


Fig. 6. Example of SEM-EDS line-scan analysis of cross-section PEO coating (1K magnification) for sample S1.

Vickers micro-hardness values were obtained as the average of 6 recorded measurements. The standard deviation was ~5-10% due to the high roughness of the films. The maximum indentation depth was no more than 10% of the films' thickness to minimize the substrate's influence on the indentation data. Figure 7 demonstrates the behavior of the friction coefficient, wear rate, and Vickers hardness for the coatings obtained in electrolytes with different compositions, compared to the AZ63 Mg alloy substrate. Figure 7(a) shows that for the samples processed through PEO, the friction coefficients are lower than the friction coefficient of the substrate, indicating that an increase in the aluminate concentration leads to a reduction in the friction coefficient, with the average values of the roughness of the protective layers being similar. It can be observed that all PEO coatings exhibit superior tribological characteristics compared to the substrate. Table VI depicts the average values measured for the three coatings and the Mg AZ63 substrate.

TABLE VI. AVERAGE MEASURED TRIBOLOGICAL PARAMETERS

Probe	Averaged friction coefficient	Specific wear rate (mm ³ /Nxm)	HV/0.5
AZ63	0.29	3.09 ± 0.15	80.00 ± 8.00
S1	0.28	0.57 ± 0.03	1150.00 ± 115.00
S2	0.27	1.14 ± 0.06	850.00 ± 85.00
S3	0.24	2.02 ± 0.10	775.00 ± 77.50

The improvement in wear resistance of the coated magnesium samples can be attributed to the high microhardness of the coatings [21]. Consequently, the volume loss resulting from wear was reduced by 5 times for the S1

sample. The adhesion strength of the prepared coatings was determined by taking three measurements for each sample, applying a progressive load in the range of 0 to 100 N, at a loading rate of 10 N/min, over a distance of 10 mm. The standard deviation of the adhesion strength was between 5 and 10%. The failure mode was defined as the characteristic load, L_c , for the delamination of more than 50% of the coating. Figure 8 displays the variation of the tribological properties of the ceramic coatings, acquired with mixed aqueous electrolytes at different aluminate concentrations. Sample S1 can be observed to exhibit the best tribological characteristics (high hardness and minimal wear rate). Tribological parameters vary inversely proportional to the increase in NaAlO_2 concentration in the electrolyte. In contrast, the coefficient of friction of the investigated surfaces decreases with increasing aluminate concentration. This reduction can be attributed to a higher presence of the hard MgAl_2O_4 phase and a greater thickness of the coatings, as the surfaces exhibit similar surface roughness values.

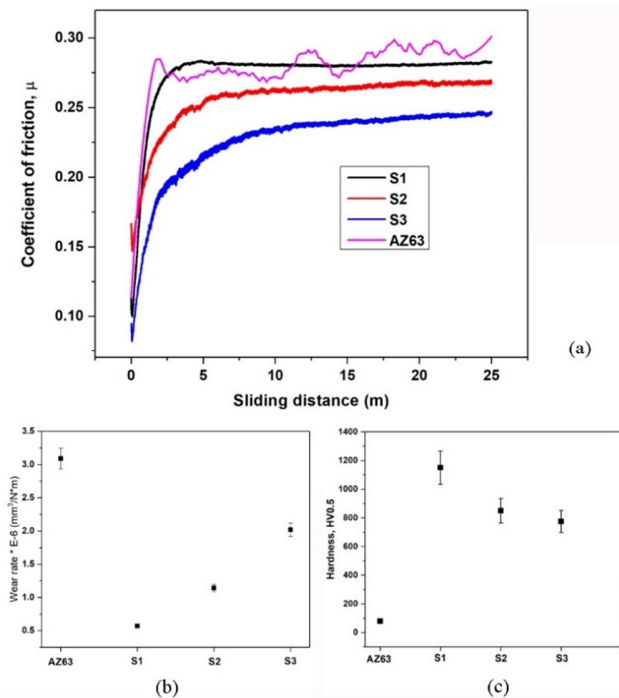


Fig. 7. Evolution of the friction coefficient (a), wear rate (b), and Vickers hardness (c) for the PEO coatings compared to the AZ63 Mg alloy substrate.

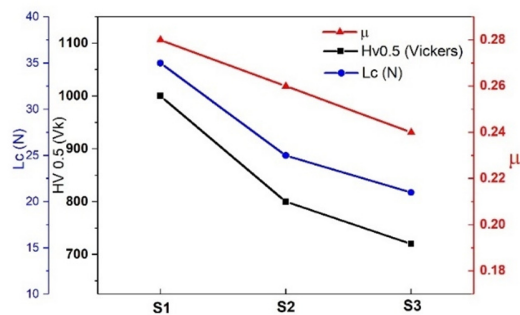


Fig. 8. Variation in coating's tribological properties.

D. Corrosion Testing

Potentiodynamic bias tests were performed on AZ63 alloys to investigate the corrosion rate variations. The anodic branch was not as steep as the cathodic branch, implying that the cathodic reaction dominated the corrosion process in all samples. All Mg alloy applications were associated with their polarization behaviors that are fundamentally governed by their electrochemical mechanism. Electrochemical corrosion of Mg is described as a reaction of Mg with water. Table VII portrays the linear potentiometry parameters in a 3.5% NaCl solution.

TABLE VII. LINEAR POTENTIOMETRY PARAMETERS

Sample	Corrosion process parameters						
	OCP (mV)	E(I=0) (mV)	i_{corr} (μA)	v_{corr} ($\mu\text{m}/\text{year}$)	R_p ($\text{kohm} \times \text{cm}^2$)	$-\beta_c$ (mV/dec)	β_a (mV/dec)
AZ63	-1530	-1429	27.5	663.6	0.33	191	43
S1	-1510	-1467	20.14	464.64	2.46	353	216
S2	-1515	-1444	2.96	68.17	8.09	152	58
S3	-1520	-1500	11.47	264.48	1.78	115	117

The OCP values are close for the AZ63 sample as well as for the coated samples, a fact attributed to the protective coating. On the other hand, the values of the corrosion current i_{corr} are lower for the coated samples compared to the AZ63 sample. This indicates that the deposited layers have a protective role and the corrosion rate decreases from 663.6 $\mu\text{m}/\text{year}$ for the AZ63 alloy to 68.17 $\mu\text{m}/\text{year}$ for the S2 sample. An increased ratio of MgAl_2O_4 to MgO was reported to enhance the corrosion resistance [22]. However, in the case of the S3 sample, an increase in the corrosion current showed a respective increase in the corrosion speed. This behavior indicates that the surface film has been attacked by the Cl ions. This can be attributed to a higher number of defects, which allowed the corrosive solution to penetrate, thus initiating substrate corrosion [12].

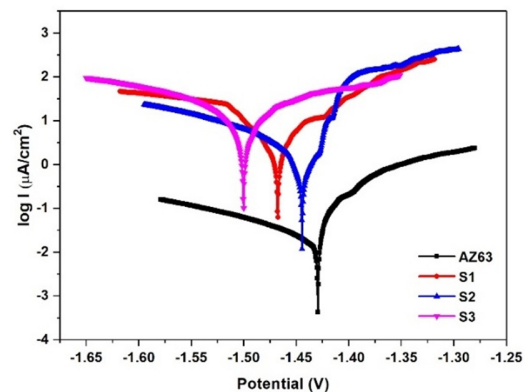


Fig. 9. Tafel representations.

Tafel representations of linear potentiometry tests are given in Figure 9. Figure 10 presents the cyclic polarization curves for the investigated materials, characteristic of alloys that corrode in points (pitting corrosion) [23]. Chlorine ions in the electrolyte can cause localized damage to the magnesium hydroxide ($\text{Mg}(\text{OH})_2$) layer, leading to pitting corrosion.

Similar behavior is also observed in the case of the covered samples but with a much lower recorded current intensity [24], indicating slower corrosion in the case of these samples subjected to oxidation compared to the initial sample.

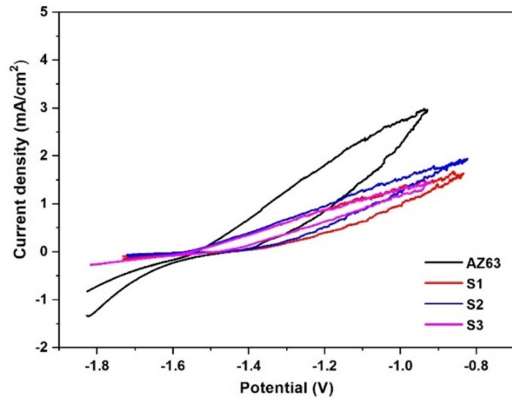


Fig. 10. Cyclic polarization curves.

Due to the 30-minute holding period before the measurements, the corrosion was initiated and a layer of Mg oxide and hydroxide was formed on the surface of the sample. For the EIS measurements, the equivalent circuit for the AZ63 alloy exhibited in Figure 11 (a) is proposed to curve-fit the measured EISs. The components/parameters of the circuit are the following: R_s is the solution resistance, R_t is the load transfer resistance, Q is the capacitance of the electric double layer, R_{LMg^+} is the induction resistance for the electrochemical reactions at the film/Mg interface, and L_{Mg^+} is the inductance for the electrochemical reactions at the film/Mg interface. A better adjustment of the data was obtained by replacing the double-layer capacity with a constant phase element, namely CPE, which expresses the non-ideal behavior of the electrical double-layer capacity (change of capacity with frequency). For the coated samples, the circuit from Figure 11 (b) was used. RL and L in series represent the low-frequency resistance and inductance resulting from the desorption of corrosion products. Table VIII presents the values of the parameters that best satisfy the experimental data.

TABLE VIII. EXPERIMENTAL DATA ADJUSTMENT PARAMETERS

Sample	R_s ($\Omega \times \text{cm}^2$)	CPE		R_t ($\Omega \times \text{cm}^2$)	R_L ($\Omega \times \text{cm}^2$)	L ($\text{H} \times \text{cm}^2$)	R_L ($\Omega \times \text{cm}^2$)	L ($\text{H} \times \text{cm}^2$)
		$Q \times 10^{-5}$ ($\text{S} \cdot \text{s}^n / \text{cm}^2$)	n					
AZ63	67	2.46	0.67	774	619	365	-	-
S1	10	1.61	0.37	5387	16570	3746	-	-
S2	70	2.29	0.43	39430	19610	2707	16110	80
S3	13	1.92	0.40	2067	3129	23700	10260	3919

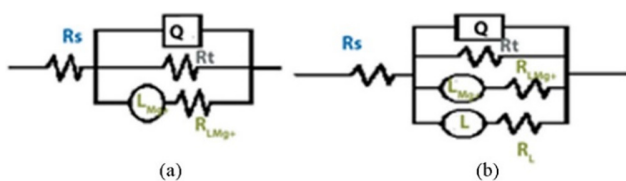


Fig. 11. Equivalent circuits for AZ63 Mg alloy (a) and coated samples (b).

In the case of the AZ63 sample, the charge transfer resistance (R_{ct}) has a relatively low value compared to the coated samples, indicating a high corrosion rate. By corroding the surface of the sample, it becomes rough, which makes the capacitance of the electrical double layer non-ideal and requires the introduction of the Constant Phase Element (CPE). The deviation of the frequency exponent value (n) from 1 is a measure of the deviation from the ideality of the capacitor that represents the capacity of the electric double layer. A continuous layer was not formed on the surface of the sample, but only ions from the solution and/or insoluble corrosion products were adsorbed. Due to this fact, the R_{L-L} series group was introduced in the equivalent circuit in parallel with the time-constant characteristic of the double layer (CPE- R_{ct}). The circuit element R_L represents the resistance as a result of the components adsorbed on the surface, and L is an inductor (coil), which in EIS describes the inductive loops in the low-frequency domain. The increase of R_t in the coated samples implies that the film becomes protective for the Mg samples. Similar variations in R_L and L are also observed. In the case of sample S3, the R_L decreases. This may occur because a larger area of the Mg substrate is exposed to the electrolyte solution or the film becomes more porous.

Figure 12 depicts the Nyquist plots of the samples, representing the dynamic characteristics of surface dissolution. The spectra are made up of a single high-frequency capacitive loop and a low-frequency inductive loop. This is because the layer progressively breaks down and corrosion products are gradually generated [25].

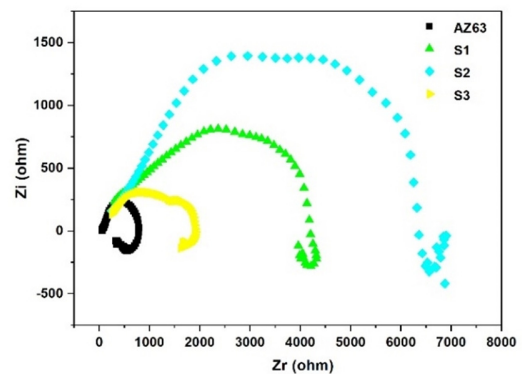


Fig. 12. Nyquist plots of the samples.

Figure 13 provides a presentation of the EIS data in a Bode plot. The impedance modulus increases for the coated samples compared to that of AZ63 in the initial state, and there is no distinct time constant in the mid-frequency range. An increase in the impedance is expected in the coated state because the surface film formed on Mg protects the surface over a period of time. Additionally, the maximum phase angle observed for all coated samples was obtained for the maximum phase angle, indicating a capacitive response for all samples and suggesting the presence of layers on the surface acting as a barrier.

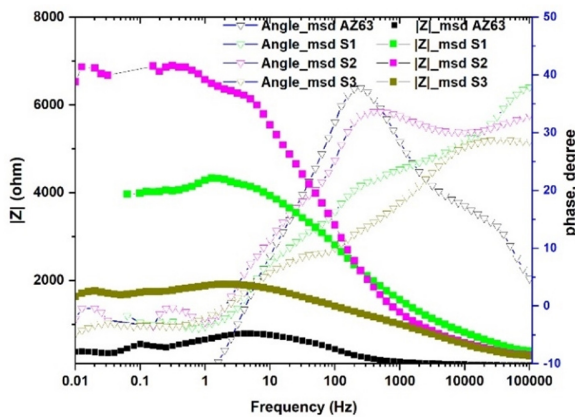


Fig. 13. Bode plot of the analyzed samples.

IV. CONCLUSION

PEO treatment in mixed aqueous electrolytes has been demonstrably successful in improving the properties of the AZ63 magnesium alloy, addressing its limitations, particularly regarding corrosion susceptibility and wear resistance. XRD analyses revealed that the three coatings share similar compositions, exhibiting a structure composed of spinel, magnesium oxide, and magnesium phosphate. The increase in sodium aluminate concentration in the electrolyte led to a quantitative increase in the spinel phase in the coatings. Similar results were presented in [15], where this phenomenon was attributed to the preferential formation of aluminum-based compounds due to the increased concentration of aluminate ions in the electrolyte. However, despite using a similar phosphate concentration (10 g/L) and a lower aluminate concentration compared to this study, no phosphate-based compound was obtained through PEO on the AM60B magnesium alloy.

Although a decrease in roughness and porosity was observed with increasing aluminate concentration from 2 to 3 g/L in a mixed aluminate-phosphate electrolyte in [17], the results of this study show that the coatings acquired exhibited typical PEO morphologies, with similar values for surface roughness and porosity regardless of the aluminate concentration in the mixed electrolytes. However, this study's findings demonstrate that the aluminate concentration directly influences the thickness of the coatings obtained proportionally, with an average thickness of 46.25 μm acquired for the electrolyte containing 25 g/L NaAlO_2 .

All samples subjected to PEO processing exhibit superior tribological characteristics compared to the substrate, with the sample obtained in the electrolyte with the lowest amount of NaAlO_2 , S1, demonstrating the highest hardness, best adhesion, and lowest wear rate. In [17], it was displayed that although the presence of spinel in the coatings enhances their properties, these coatings exhibit a very thin outer layer. Therefore, a balanced ratio between the magnesium phosphate and aluminate phases offers the best mechanical properties. On the contrary, sample S3 exhibited the lowest friction coefficient.

Impedance studies suggest that the formation of oxide layers is a multi-step reaction process involving intermediates

adsorbed on the surface that were produced by the charge transfer reaction during the corrosion process. In the Nyquist and Bode representations, a better resistance of sample S2 was observed, by both the higher values of the capacitive loop at high frequency and the large value of the impedance in this case. In the Nyquist representation, the low value of the inductive loop of this sample indicates that the absorption process is smaller. As reported in [15], the coating formed in higher NaAlO_2 concentration within the electrolyte shows better corrosion protection properties, as long as the coating is uniform and defect-free. For sample S3 obtained with the highest aluminate concentration in the electrolyte (25 g/L), the structural defects resulting from more intense discharges caused by increased electrical conductivity of the electrolyte reduced the corrosion resistance of the obtained layer.

Based on the results for the PEO of AZ63 magnesium alloys, in simple electrolytes and different processing times, and the findings presented in this study for the PEO processing in mixed electrolytes, future research will focus on studying the influence of other important process parameters on the functional properties of PEO coatings, such as current density and different unipolar and bipolar working regimes.

REFERENCES

- [1] P. Fernández-López, S. A. Alves, J. T. San-Jose, E. Gutierrez-Berasategui, and R. Bayón, "Plasma Electrolytic Oxidation (PEO) as a Promising Technology for the Development of High-Performance Coatings on Cast Al-Si Alloys: A Review," *Coatings*, vol. 14, no. 2, 2024, <https://doi.org/10.3390/coatings14020217>.
- [2] I. Patrascu, M. C. Ducu, A. D. Negrea, S. G. Moga, and A. G. Plaiasu, "Overview on plasma electrolytic oxidation of magnesium alloys for medical and engineering applications," *IOP Conference Series: Materials Science and Engineering*, vol. 1251, no. 1, Apr. 2022, Art. no. 012001, <https://doi.org/10.1088/1757-899X/1251/1/012001>.
- [3] M. M. Dicu, M. Abrudeanu, S. Moga, D. Negrea, V. Andrei, and C. Ducu, "Preparation of ceramic coatings on titanium formed by micro-arc oxidation method for biomedical application," *Journal of Optoelectronics and Advanced Materials*, vol. 14, pp. 125–130, Feb. 2012.
- [4] Z. Le, Z. Liu, X. He, Y. Cheng, P. Hu, and Y. Cheng, "Influence of Cathodic Polarization on Plasma Electrolytic Oxidation of Magnesium and AZ31 and AZ91 Magnesium Alloys," *Coatings*, vol. 13, no. 10, 2023, <https://doi.org/10.3390/coatings13101736>.
- [5] R. Cai, C. Zhao, and X. Nie, "Effect of plasma electrolytic oxidation process on surface characteristics and tribological behavior," *Surface and Coatings Technology*, vol. 375, pp. 824–832, Oct. 2019, <https://doi.org/10.1016/j.surfcoat.2019.06.104>.
- [6] Q. Huang *et al.*, "Corrosion-resistant plasma electrolytic oxidation coating modified by Zinc phosphate and self-healing mechanism in the salt-spray environment," *Surface and Coatings Technology*, vol. 384, Feb. 2020, Art. no. 125321, <https://doi.org/10.1016/j.surfcoat.2019.125321>.
- [7] C. Bertuccioli, A. Garzoni, C. Martini, A. Morri, and G. Rondelli, "Plasma Electrolytic Oxidation (PEO) Layers from Silicate/Phosphate Baths on Ti-6Al-4V for Biomedical Components: Influence of Deposition Conditions and Surface Finishing on Dry Sliding Behaviour," *Coatings*, vol. 9, no. 10, 2019, <https://doi.org/10.3390/coatings9100614>.
- [8] L. Xu, X. Liu, K. Sun, R. Fu, and G. Wang, "Corrosion Behavior in Magnesium-Based Alloys for Biomedical Applications," *Materials*, vol. 15, no. 7, 2022, <https://doi.org/10.3390/ma15072613>.
- [9] E. R. I. Mahmoud and H. F. El-Labban, "Microstructure and Wear Behavior of TiC Coating Deposited on Spheroidized Graphite Cast Iron Using Laser Surfacing," *Engineering, Technology & Applied Science*

- Research, vol. 4, no. 5, pp. 696–701, Oct. 2014, <https://doi.org/10.48084/etasr.483>.
- [10] G. Elmansouri, I. H. Kara, H. Ahlatci, and Y. Turen, "The Immersion Corrosion Resistance of Shot Peening and MAO Applied on AZ31–0.5% La Sheets," *Engineering, Technology & Applied Science Research*, vol. 10, no. 1, pp. 5201–5204, Feb. 2020, <https://doi.org/10.48084/etasr.3275>.
- [11] K. Touileb, R. Djoudjou, and A. Ouis, "Effect of Viscosity on the GTA Welds Bead Penetration in Relation with Surface Tension Elements," *Engineering, Technology & Applied Science Research*, vol. 6, no. 2, pp. 952–955, Apr. 2016, <https://doi.org/10.48084/etasr.643>.
- [12] G. Barati Darband, M. Aliofkhaeaei, P. Hamghalam, and N. Valizade, "Plasma electrolytic oxidation of magnesium and its alloys: Mechanism, properties and applications," *Journal of Magnesium and Alloys*, vol. 5, no. 1, pp. 74–132, Mar. 2017, <https://doi.org/10.1016/j.jma.2017.02.004>.
- [13] S. G. Moga *et al.*, "The Influence of Processing Time on Morphology, Structure and Functional Properties of PEO Coatings on AZ63 Magnesium Alloy," *Applied Sciences*, vol. 12, no. 24, 2022, <https://doi.org/10.3390/app122412848>.
- [14] S. Moga *et al.*, "Mechanical and corrosion-resistant coatings prepared on AZ63 Mg alloy by plasma electrolytic oxidation," *Surface and Coatings Technology*, vol. 462, Jun. 2023, Art. no. 129464, <https://doi.org/10.1016/j.surfcoat.2023.129464>.
- [15] J. Liang *et al.*, "Effects of NaAlO₂ on structure and corrosion resistance of microarc oxidation coatings formed on AM60B magnesium alloy in phosphate–KOH electrolyte," *Surface and Coatings Technology*, vol. 199, no. 2, pp. 121–126, Sep. 2005, <https://doi.org/10.1016/j.surfcoat.2005.03.020>.
- [16] S. P. Sah, Y. Aoki, and H. Habazaki, "Influence of Phosphate Concentration on Plasma Electrolytic Oxidation of AZ80 Magnesium Alloy in Alkaline Aluminate Solution," *Materials Transactions*, vol. 51, no. 1, pp. 94–102, 2010, <https://doi.org/10.2320/matertrans.M2009226>.
- [17] P. Xie *et al.*, "Effect of low concentration electrolytes on the formation and corrosion resistance of PEO coatings on AM50 magnesium alloy," *Journal of Magnesium and Alloys*, Jan. 2024, <https://doi.org/10.1016/j.jma.2024.01.020>.
- [18] V. Malinovski *et al.*, "Improvement of Mechanical and Corrosion Properties of Commercially Pure Titanium Using Alumina PEO Coatings," *Coatings*, vol. 12, no. 1, 2022, <https://doi.org/10.3390/coatings12010029>.
- [19] F. Wei, W. Zhang, T. Zhang, and F. Wang, "Effect of variations of Al content on microstructure and corrosion resistance of PEO coatings on MgAl alloys," *Journal of Alloys and Compounds*, vol. 690, pp. 195–205, Jan. 2017, <https://doi.org/10.1016/j.jallcom.2016.08.111>.
- [20] J. F. Archard, "Contact and Rubbing of Flat Surfaces," *Journal of Applied Physics*, vol. 24, no. 8, pp. 981–988, Aug. 1953, <https://doi.org/10.1063/1.1721448>.
- [21] X. Li, X. Liu, and B. L. Luan, "Corrosion and wear properties of PEO coatings formed on AM60B alloy in NaAlO₂ electrolytes," *Applied Surface Science*, vol. 257, no. 21, pp. 9135–9141, Aug. 2011, <https://doi.org/10.1016/j.apsusc.2011.05.115>.
- [22] Y. Ma, X. Nie, D. O. Northwood, and H. Hu, "Systematic study of the electrolytic plasma oxidation process on a Mg alloy for corrosion protection," *Thin Solid Films*, vol. 494, no. 1, pp. 296–301, Jan. 2006, <https://doi.org/10.1016/j.tsf.2005.08.156>.
- [23] M. G. Zaharia, S. Stanciu, R. Cimpoesu, I. Ionita, and N. Cimpoesu, "Preliminary results on effect of H₂S on P265GH commercial material for natural gases and petroleum transportation," *Applied Surface Science*, vol. 438, pp. 20–32, Apr. 2018, <https://doi.org/10.1016/j.apsusc.2017.10.093>.
- [24] J. Izquierdo, G. Bolat, N. Cimpoesu, L. C. Trinca, D. Mareci, and R. M. Souto, "Electrochemical characterization of pulsed layer deposited hydroxyapatite-zirconia layers on Ti-21Nb-15Ta-6Zr alloy for biomedical application," *Applied Surface Science*, vol. 385, pp. 368–378, Nov. 2016, <https://doi.org/10.1016/j.apsusc.2016.05.130>.
- [25] J. Li, Q. Jiang, H. Sun, and Y. Li, "Effect of heat treatment on corrosion behavior of AZ63 magnesium alloy in 3.5 wt.% sodium chloride solution," *Corrosion Science*, vol. 111, pp. 288–301, Oct. 2016, <https://doi.org/10.1016/j.corsci.2016.05.019>.